Discriminating Lattice Structural Effects from Electronic Contributions to the Superconductivity of Doped MgB_2 with Nanotechnology

Sean Li,*,†,‡ T. White,‡ C. Q. Sun,‡ Y. Q. Fu,‡ J. Plevert,‡ and K. Lauren§

School of Materials Science and Engineering, The University of New South Wales, NSW 2052, Australia, School of Materials Engineering, Nanyang Technological University, Singapore, and Department of Chemical Engineering, Kyoto University, Kyoto 615-8510, Japan

Received: May 16, 2004; In Final Form: June 29, 2004

Most partial altervalent/aliovalent substitutions for Mg or B in MgB_2 studied to date depress the superconducting transition temperature (T_c) and, at higher replacements, completely suppress superconductivity of MgB_2. The diminution and loss of superconductivity in MgB_2 arise from the subtle interplay between the competing/cooperating effects of the electronic and lattice structural variations, which are induced by the different charge and atomic radii of the substituents. Here, we experimentally discriminate lattice structural effects from electronic contributions to superconductivity by exploiting the nanosize dependence of the lattice structure to modify structural parameters without resorting to chemical doping. It is found that the superconductivity of MgB_2 is extremely sensitive to lattice parameter variation, such that contraction of Mg−Mg bond dramatically depresses T_c and eventually results in the loss of superconductivity as the average coordination of Mg to B falls from 12 to 8 due to the introduction of B vacancies for nanocrystalline MgB_2 of 2.5 nm diameter.

Introduction

The discovery of a superconducting transition at 39 K in MgB_2 initiated enormous scientific interest both to understand the phenomenon and to exploit its remarkable intrinsic performance for magnetic and electronic applications.[1,2] The BCS electron−phonon model and the two-gap model are two theoretical frameworks proposed to explain high-temperature superconductivity observed in MgB_2.[3,4] On the basis of these models, partial altervalent/aliovalent chemical substitutions for Mg or B have been attempted to (1) modify the Fermi-level density-of-states with minimum disruption of the electronic network and (2) alter the lattice parameters, thus varying the superconducting transition temperature (T_c).[5−11] However, most of the substitutions studied to date depress T_c and at higher replacements completely suppress the superconductivity of MgB_2. This behavior is different from that of Cu oxide superconductors, in which replacement of La by Y in La_2CuO_4 forms $YBa_2Cu_3O_{7-\delta}$ and raises T_c from 35 to 93 K. It suggests that the diminution and loss of superconductivity in MgB_2 arises from the subtle interplay between the competing/cooperating effects of the electronic and lattice structural variations, which are induced by the different charge and atomic radii of the substituents. To understand these effects, it is necessary to isolate the electronic and crystallographic contributions to superconductivity to arrive at a fundamental understanding of observed T_c suppression behaviors and also the mechanism of superconductivity. It is generally true that the lattice constants of bulk materials are modified as crystal sizes approach nanoscales, resulting in bond length and angle variation and, in extreme cases, changes in atomic coordination numbers (CN). This intrinsic structural behavior of nanomaterial lattices allows the structural parameters of MgB_2 to be modified without resorting to chemical doping. In this work, we employ this unique behavior of nanomaterials to discriminate lattice structural effects from electronic contributions to investigate the dominant parameters of superconducting transition behavior in MgB_2.

Experimental Section

Recently, hydrostatic pressure was employed to determine the lattice compressibility of MgB_2 and its effects on T_c. It was found that T_c decreased from 39 to 30.5 K with increasing pressure up to 10 GPa.[12] However, pressure and temperature are intensive variables of a thermodynamic system, and any adjustment of these may result in phase changes that strongly influence the superconductivity, as evidenced by its appearance in iron, boron, lithium, and platinum at high hydrostatic pressure. It is usually thought that the application of external pressure leads only to a limited compression of lattice parameters, which is insufficient to cause changes in coordination number.

An alternative method to precisely modify lattice structural parameters, while avoiding possible complications induced by temperature and pressure, is physical reduction of crystal size through ball-milling MgB_2 (99% purity, Aldrich) in tungsten carbide (WC) bowls purged with Ar. A continuous cycle of 5 min of milling and 3 min of rest time was programmed to minimize heat accumulation. In this manner, highly reproducible size reduction could be achieved as a function of milling time. Powder X-ray diffraction (XRD) patterns were collected by use of Cu Kα radiation with step-scanning in the 2θ range 20°−60° at intervals of 0.02°. Peak position was calibrated by spiking with 5 wt % Si (NIST 640c). Rietveld analysis was carried out by a fundamental parameter procedure as implemented on TOPAS R (version 2.1) to determine lattice parameters and quantitatively extract phase contents. The MgB_2 starting model used in the refinement was that of Russell et al.[13] In each case, a background polynomial, scale factor, cell parameters, zero-point correction, and sample displacement were refined. All atoms were on special positions, isotropic thermal parameters

* Corresponding author: e-mail assxli@ntu.edu.sg.
† The University of New South Wales.
‡ Nanyang Technological University.
§ Kyoto University.

10.1021/jp047902x CCC: $27.50 © 2004 American Chemical Society
Published on Web 09/29/2004

TABLE 1: Structural Parameters as a Function of Crystal Size in MgB_2

size (nm)	T_c (K)	cell volume (Å^3)	a axis (Mg−Mg) (Å)	c axis (Å)	B−B bond[a] (Å)	Mg−B bond[b] (Å)	B−Mg−B angle[c] (deg)	Mg−B−Mg angle[d] (deg)
64.1	39.2	29.06	3.0864(2)	3.5226(2)	1.7819(1)	2.5055(1)	41.67	76.04
19.7	39.2	29.08	3.0866(4)	3.5452(6)	1.7821(2)	2.5062(3)	41.66	76.02
11.8	39.2	29.10	3.0867(6)	3.6266(10)	1.7821(2)	2.5070(4)	41.65	75.99
7.7	29.6	29.12	3.0863(8)	3.5299(13)	1.7819(3)	2.5080(5)	41.62	75.95
6.2	21.8	28.95	3.0746(12)	3.5363(20)	1.7751(5)	2.5055(8)	41.50	75.70
4	13.2	28.88	3.0735(14)	3.5303(24)	1.7745(6)	2.5029(10)	41.53	75.76
2.5	0	28.09	3.0505(27)	3.4853(44)	1.7612(11)	2.4776(19)	41.65	75.99

[a] $a/\sqrt{3}$. [b] $[(c/2)^2 + (a/\sqrt{3})^2]^{1/2}$. [c] $2\{\sin^{-1}[[(a/\sqrt{3})/2]/[[(c/2)^2 + (a/3)^2]^{1/2}]\}$. [d] $2\{\sin^{-1}[(a/2)/[[(c/2)^2 + (a/\sqrt{3})^2]^{1/2}]\}$.

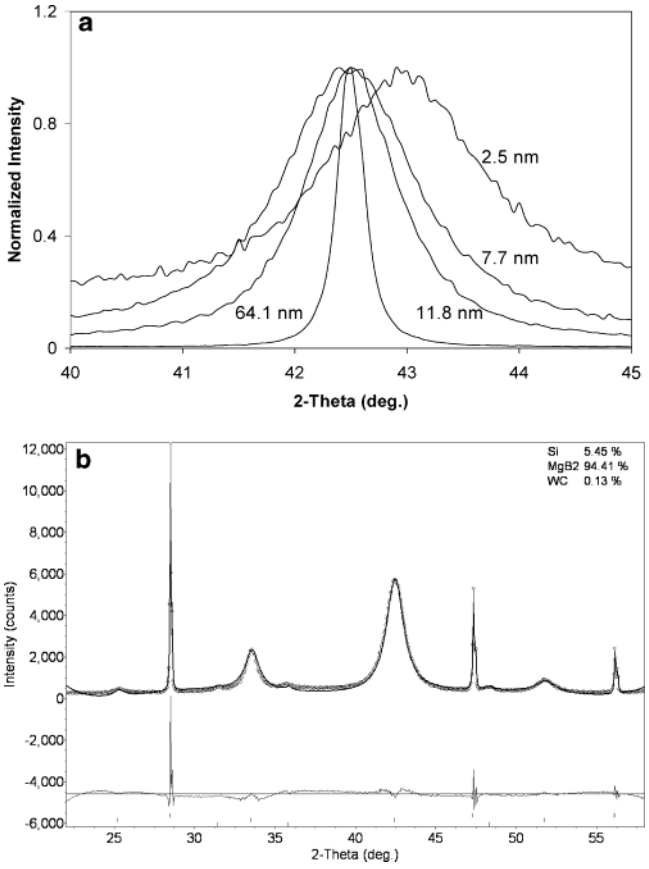

Figure 1. (a, top panel) Normalized MgB_2 (101) peaks show peak broadening with crystal size reducing. (b, bottom panel) Final fit between calculated (—) and experimental (○) diffraction profiles for MgB_2 of 7.7 nm. Bragg markers from top to bottom are Si, MgB_2, and WC.

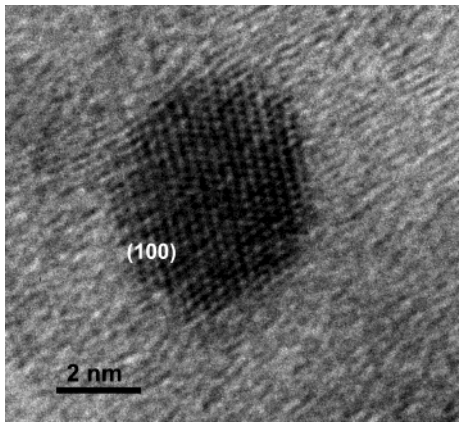

Figure 2. HRTEM morphology shows single-crystal MgB_2 of a particle; such crystals with ~10% size deviation are uniformly distributed in the samples.

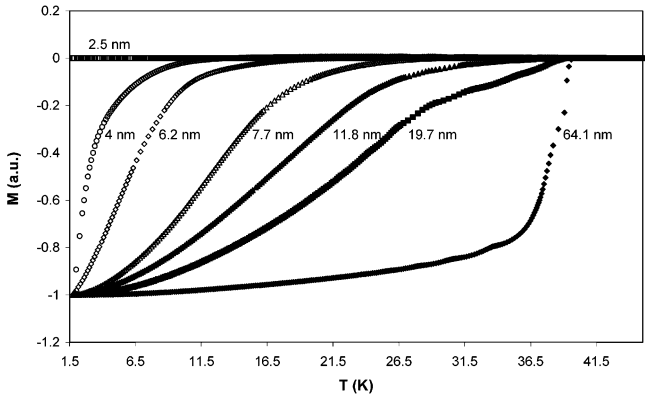

Figure 3. Magnetic moments as a function of temperature, showing size dependence of superconducting transition temperature of MgB_2. T_c is invariant with the reduction of crystal sizes from 64.1 to 11.8 nm but dramatically decreases to 13.2 K as the crystal size is further reduced to 4 nm. For the smallest crystals of MgB_2 (2.5 nm), superconductivity is completely lost.

were fixed (1 Å^2), and crystal sizes were extracted from the (100), (101), and (002) peaks. For the smallest crystals (i.e., longest milling times), the site occupancy of B was refined. Secondary phases (tungsten carbide and silicon) were included by use of appropriate starting models. During milling, the peak width of MgB_2 reflections increased as the size of the diffracting crystals decreased (Figure 1a). In addition, mechanical contamination from unreacted WC with less than 1 wt % was detected in samples with the longest milling durations and was starkly evident due to low intensity of MgB_2 reflections. A typical Rietveld match is shown in Figure 1b. In this manner, accurate cell constants were derived from which bond lengths and angles could be derived with high precision (Table 1). High-resolution transmission electron microscopy (HRTEM) was employed to verify the crystal sizes determined by XRD. Quantitative analysis showed that, except for size variation and modulation of structural parameters, no other chemical reactions occurred during the milling process. To assess the influence of WC on T_c of MgB_2, a standard sample containing 99 vol % MgB_2 + 1 vol % WC was prepared and shown to have no influence on superconducting transition temperature. To increase the sensitivity in AC susceptibility measurement, the applied background field was lowered to 1 Oe. For all samples, magnetic moment (Am^2) as a function of temperature was measured for loose powders (0.1 g) with Oxford MagLab Systems by zero-field cooling.

Results and Discussion

Commercial MgB_2 is composed of 1 μm polycrystalline particles with a crystal size of 64.1 nm. The first effect of physical reduction in particle/crystal size is to destroy the intercrystallite coupling to produce isolated nanosized single crystals (Figure 2). Figure 3 plots magnetic moments as a

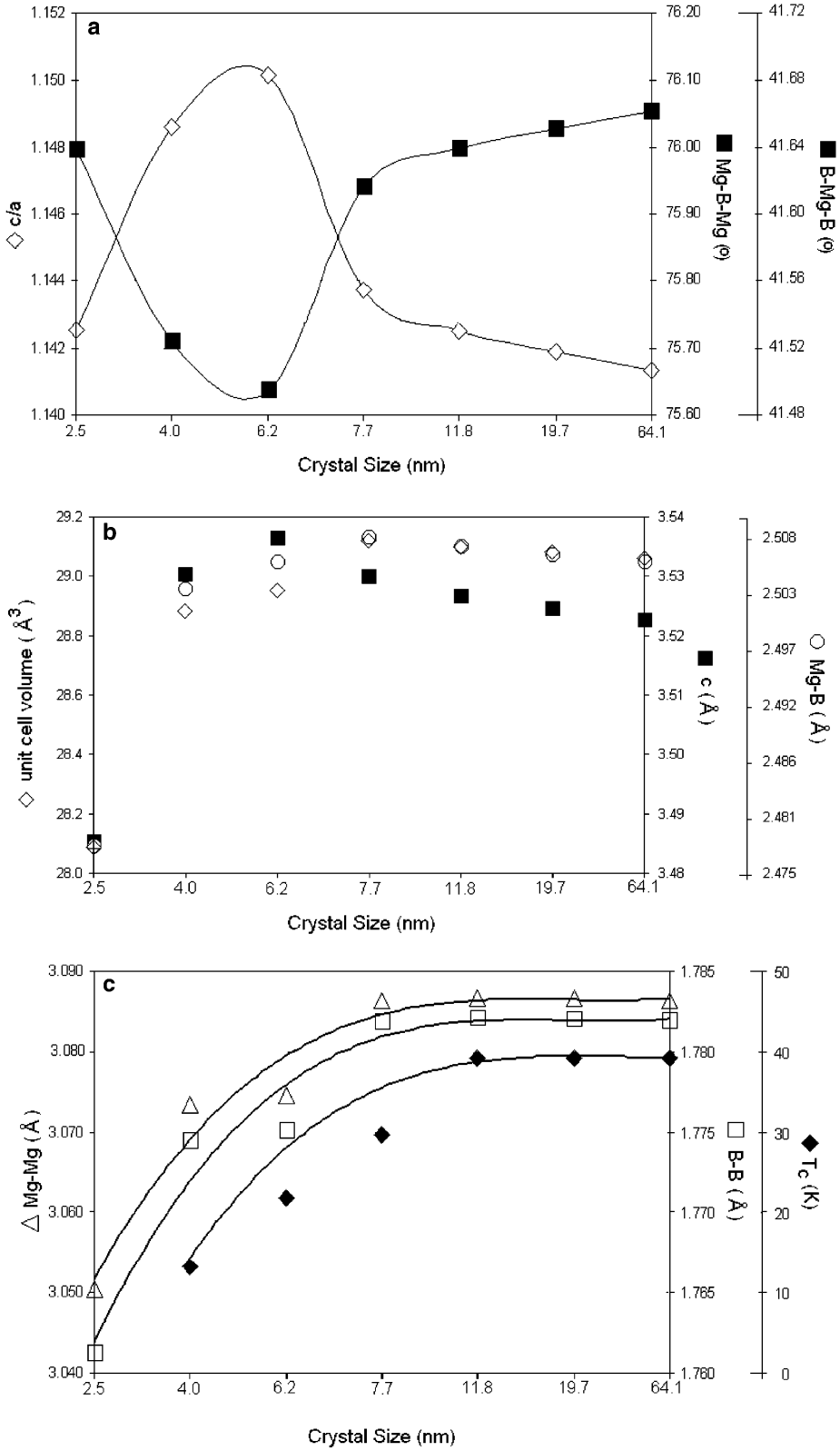

Figure 4. The variation trends of (a, top panel) cell volume, *c*-axis, Mg−B bond length, and (b, middle panel) Mg−B−Mg and B−Mg−B angles do not correlate with T_c, suggesting these factors do not directly influence the transition temperature. (c, bottom panel) Variations of Mg−Mg and B−B bonds have similar trends of T_c variation, implying that Mg−Mg and B−B bonds are the critical structural parameters that correlate with T_c. Errors are given in Table 1.

function of temperature for the as-prepared nanocrystalline MgB_2 materials. There is a size dependence of T_c (the temperature of transition onset) that is invariant for crystal sizes from 64.1 to 11.8 nm but dramatically decreases to 13.2 K for the crystals below 11.8 nm. For the smallest crystals (2.5 nm), superconductivity is completely lost. In a crystallochemical sense, MgB_2 can be described as the intergrowth of a 6^3 (graphitelike) planar net of B intercalated between a 3^6 net of Mg. The Mg 3^6 net describes hexagonal close packing (hcp) and corresponds to the parent metal Mg structure. For the as-prepared MgB_2 materials, structural parameters as a function of crystal size are listed in Table 1 and plotted in Figure 4. The

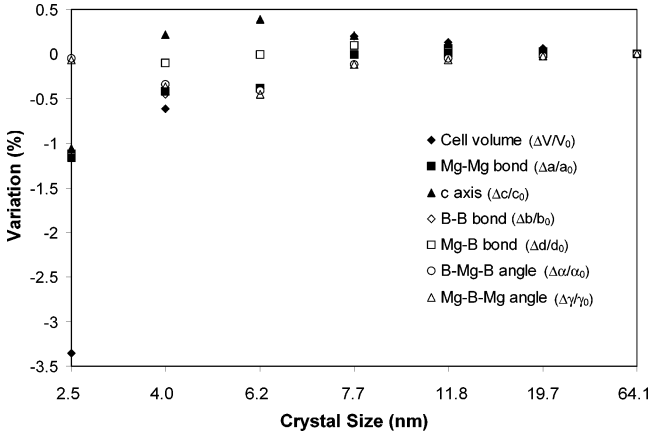

Figure 5. Crystal size dependence of variation percentages for the structural parameters.

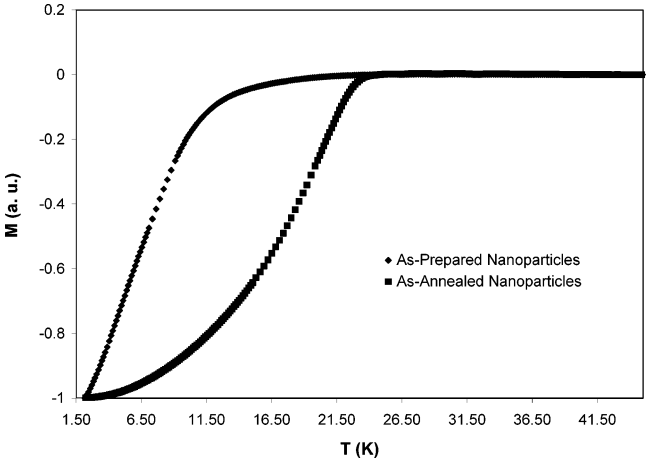

Figure 6. Magnetic moments as a function of temperature for the as-prepared nanocrystalline MgB_2 of 6.2 nm, measured before and after annealing at 550 °C for 1 h. The annealing was conducted to release the microstress and strain, and the results show that microstrain induced by the milling process has limited influence on T_c but broadens the transition.

geometry of the structural parameters requires that B−Mg−B and Mg−B−Mg bond angles change cooperatively. From Figure 4a,b, it can be clearly seen that the trends of cell volume, *c*-axis, Mg−B bond length, and B−Mg−B and Mg−B−Mg bond angles do not correlate with T_c, suggesting these factors are not directly influencing the transition temperature. The *P*622 symmetry of MgB_2 constrains the Mg−Mg−Mg and B−B−B angles to 120°, thereby maintaining perfect Mg 3^6 and B 6^3 subnets regardless of crystal size, so these features cannot be responsible for the depression of T_c. However, Mg−Mg and B−B bond lengths trend with T_c, which is almost independent of crystal size from 64.1 to 11.8 nm but decreases dramatically below 11.8 nm (Figure 4c). This implies that Mg−Mg and B−B bonds are the critical structural parameters that correlate with T_c. These results, and the trend of the Mg−Mg bond length effect on T_c, are in agreement with the results obtained by hydrostatic pressure experiments,[12] although the effect of hydrostatic pressure was weaker. The weak effect may be correlated with the change of thermodynamic condition by varying the pressure.

It is difficult to separate the individual contributions from Mg−Mg ($=a$) and B−B ($= a/\sqrt{3}$) bonds to T_c as they are geometrically linked to the *a*-parameter and independent of the *c*-axis. However, for the smallest crystals, the relative Bragg intensities can only be successfully matched during Rietveld refinement through the introduction of statistically distributed B-vacancies, with the refined value falling from 1 to $^2/_3$. In other words, the average coordination of Mg to B falls from 12 to 8, resulting in the loss of superconductivity. As expected from geometry, the Mg−Mg bond has similar nanosize dependence of relative variation percentage with B−B bond (Figure 5), but Mg retains full occupancy regardless the crystal size. It has been reported elsewhere that the contraction of Mg−Mg bonds will be limited due to the need to maintain a reasonable B−B distance.[14] Our results suggest that for small crystals (<4 nm) Mg−Mg bond shortening can be accommodated through the introduction of B vacancies. Therefore, statistical occupation of the B-site allows the Mg−Mg bond to contract further than might otherwise be possible, and this distance is the primary determinant of T_c in MgB_2. This result is also in agreement with the theoretical prediction of 7 nm by the bond order−length−strength correlation mechanism.[15]

In addition to lattice variations, the effect of lattice strain on T_c, induced by the milling process, must also be considered. As MgB_2 is a brittle intermetallic compound, most of the mechanical energy applied during milling is converted to fracture energy to diminish the crystal size. It has been demonstrated that 5% displacement per atom induced by proton irradiation only leads to the depression of T_c in 2 K.[16] The maximum microstrain measured from the as-prepared samples by XRD refinement is less than 0.2%, which exists in the smallest crystals (2.5 nm), and it is too small to influence T_c significantly. Figure 6 plots magnetic moments as a function of temperature for MgB_2 of 6.2 nm before and after annealing at 550 °C for 1 h. This experiment, conducted to release the microstress and strain, shows no remarkable change in T_c. However, the transition profile was altered from a concave to a convex curve by annealing. It demonstrates that microstrain induced by the milling process only broadens the transition but has limited influence on the transition temperature. Furthermore, the depressed T_c was restored by annealing the as-prepared material at 950 °C for 4 h through recrystallization, crystal growth, and sintering. This result provides evidence that no chemical reactions occurred during the milling process, as the result in quantitative analysis with Rietveld refinement, and the mechanical contamination does not influence the T_c. It also further supports the notion that the dramatic reduction of T_c is a consequence of Mg−Mg bond contraction with size reduction and is in good agreement with independent studies that showed a pressure dependence of T_c in MgB_2.[12]

T_c depression and suppression have also been observed in altervalent/aliovalent chemically substituted MgB_2 materials. T_c is depressed significantly with addition of Al in $Mg_{1-x}Al_xB_2$ and the superconductivity is lost at $x = 0.4$ (Figure 7).[5] The association of Al substitution is subtle and complex, with physical properties determined by the interplay of both electron and lattice structures. In $Mg_{1-x}Al_xB_2$, the *a*-axis (Mg−Mg bond) contracts from 3.083 to 3.055 Å, while the contraction of *c*-axis is from 3.526 to 3.367 Å, as *x* increases from 0 to 0.4.[6] Although the variation of *c*-axis in $Mg_{0.6}Al_{0.4}B_2$ is greater than that in the nanocrystalline MgB_2 of 2.5 nm, the lengths of their Mg−Mg bonds are similar. This suggests that the loss of superconductivity in $Mg_{0.6}Al_{0.4}B_2$ may be a result of the Mg−Mg bond contraction caused by smaller Al. Except for the electron doping in $Mg_{1-x}Al_xB_2$, the hole doping with cation substitution of Li for Mg in $Mg_{1-x}Li_xB_2$ also depresses T_c in a similar way as the contraction of the Mg−Mg bond (Figure 7).[7] The significance of the Mg−Mg bond effects on T_c can also be found in MgB_2, where B is partially replaced by Be (hole doping) and C (electron doping). Although the *c*-axis increases as Be increases

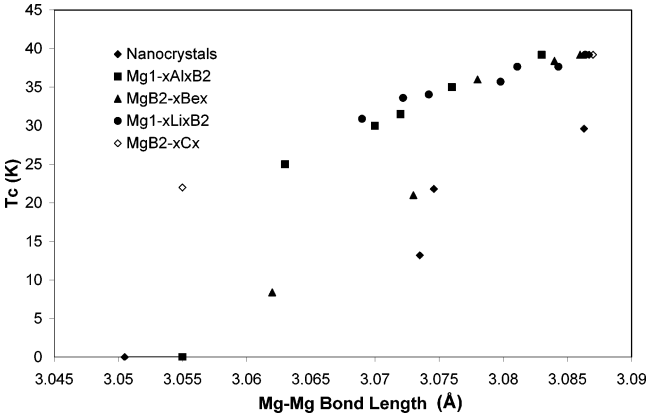

Figure 7. Similar behavior in Mg−Mg bond length dependence of T_c, supporting the notion that the superconductivity of MgB_2 is highly sensitive to lattice structure and the Mg−Mg bond dominates the superconducting transition behavior.

from $x = 0$ to 0.6 in $MgB_{2-x}Be_x$, the Mg−Mg bond decreases from 3.084 to 3.062 Å, resulting in T_c depressing from 38.4 to 8.4 K.[8] Similarly, the T_c of C-doped MgB_2 decreases by 17 K as the Mg−Mg bond contracts from 3.87 to 3.055 Å while the *c*-axis remains unchanged in $Mg(B_{0.8}C_{0.2})_2$.[9,10] It is of interest that superconductivity is retained in $Mg(B_{0.8}C_{0.2})_2$ when the Mg−Mg bond length is 3.055 Å, although this leads to the loss of superconductivity in the Al-doped materials and the nanocrystalline MgB_2 of 2.5 nm. This may be due to the different nature of the replacements in Mg and B sites. The substitution of C for B changes the charge distribution of σ-bonding states in the B planes that couple very strongly to the in-plane vibration of B atoms. Therefore, such a substitution affects strong-electron-pair formation of the σ-bonding states, which is crucial to the appearance of superconductivtiy in MgB_2.[4,17] It was proposed that the transition temperature might increase in this layered material by C partially filled planar orbital.[4] Although there is no direct experimental evidence for the proposition above, it is clear that the 17 K reduction of T_c in $Mg(B_{0.8}C_{0.2})_2$ has contributions from competing/cooperating effects of electronic and lattice structures caused by the C doping. In this case, the individual contribution from electronic effects may partially compensate the lattice effects on T_c to yield different results as compared to the Al-doped and nanocrystalline MgB_2. Regardless of the doping mechanisms and the atomic replacements, the experiments show that T_c is depressed whenever the Mg−Mg bond contracts, indicating that (1) the superconductivity of MgB_2 is highly sensitive to lattice structure, (2) the Mg−Mg bond dominates the superconducting transition behavior, and (3) increasing T_c of MgB_2 may not be readily achieved by varying the Fermi-level density-of-states through chemical doping. To gain a better understanding in the atomic parameter effects on T_c of MgB_2, a comparative study on elemental superconductors, such as niobium etc., is being performed and the results will be reported in the near future.

Conclusion

The dominant factors influencing superconducting transition behavior of doped MgB_2 have been investigated by the discriminating lattice structural effects from electronic contributions to superconductivity through utilization of the intrinsic structural behavior of nanocrystalline materials. The results suggest that increasing T_c may not be easily achieved by the partial altervalent/aliovalent substitution for Mg or B, if such substitutions simultaneously lead to a contraction of the Mg−Mg bond even though favorable modification of the Fermi-level density-of-states occurs. It would appear that the superconductivity of MgB_2 is extremely sensitive to its lattice constants, especially as these reflect contraction of Mg−Mg bond and the simultaneous depression of T_c. Further shortening of the Mg−Mg bond eventually results in the loss of superconductivity by the average coordination of Mg to B falling from 12 to 8. As T_c is depressed as the crystal size falls below 11.8 nm and completely suppressed at 2.5 nm, improvements in the high-field performance of MgB_2 through minimization of crystal size[18] may be limited by the size dependence of transition behavior of MgB_2.

References and Notes

(1) Nagamatsu, J.; Nakagawa, N.; Muranaka, T.; Zenitani, Y.; Akimitsu, J. *Nature* **2001**, *410*, 63.

(2) Larbalestier, D.; Gurevich, A.; Feldmann, D. M.; Polyanskii, A. *Nature* **2001**, *414*, 368.

(3) Kortus, J.; Mazin, I. I.; Belashchenko, K. D.; Antropov, V. P.; Boyer, L. L. *Phys. Rev. Lett.* **2001**, *86*, 4656.

(4) Choi, H. J.; Roundy, D.; Sun, H.; Cohen; M. L.; Louie, S. G. *Nature* **2002**, *418*, 758.

(5) Slusky, J. S.; Rogado, N.; Regan, K. A.; Hayward, M. A.; Khalifah, P.; He, T.; Inumaru, K.; Loureiro, S. M.; Haas, M. K.; Zandbergen, H. W.; Cava, R. J. *Nature* **2001**, *410*, 343.

(6) de la Peña, O.; Aguayo, A.; de Coss, R. *Phys. Rev. B* **2002**, *66*, 012511.

(7) Zhao, Y.G.; Zhang, X. P.; Qiao, P. T.; Zhang, H. T.; Jia, S. L.; Cao, B. S.; Zhu, M. H.; Han, Z. H.; Wang, X. L.; Gu, B. L. *Physica C* **2001**, *361*, 91.

(8) Ahn, J. S.; Choi, E. S.; Kang, W.; Singh, D. J.; Han, M.; Choi, E. J. *Phys. Rev. B* **2002**, *65*, 2145341.

(9) Mickelson, W.; Cumings, J.; Han, W. Q.; Zettl, A. *Phys. Rev. B* **2002**, *65*, 052505.

(10) Ribeiro, R. A.; Bud'ko, S. L.; Petrovic, C.; Canfield, P. C. *Physica C* **2003**, *384*, 227.

(11) Profeta, G.; Continenza, A.; Floris, A.; Massidda, S. *Phys. Rev. B* **2003**, *67*, 1745101.

(12) Tang, J.; Qin, L. C.; Matsushita, A.; Takano, Y.; Togano, K.; Kito, H.; Ihara, H. *Phys. Rev. B* **2001**, *64*, 132509.

(13) Russell, V.; Hirst, R.; Kanda, F. A.; King, A. J. *Acta Crystallogr*. **1953**, *6*, 870.

(14) Vegas, A. *Crystallogr. Rev.* **2000**, *7*, 189.

(15) Sun, C. Q.; Zhong, W. H.; Li, S.; Tay, B. K.; Bai, H. L.; Jiang, E. Y. *J. Phys. Chem. B* **2004**, *108*, 1080.

(16) Bugoslavsky, Y.; Cohen, L. F.; Perkins, G. K.; Polichetti, M.; Tate, T. J.; Gwilliam, R.; Caplin, A. D. *Nature* **2001**, *411*, 561.

(17) Souma, S.; Machida, Y.; Sato, T.; Takahashi, T.; Matsui, H.; Wang, S. C.; Ding, H.; Kaminski, A.; Campuzano, J. C., Sasaki, S.; Kadowaki, K. *Nature* **2003**, *423*, 65.

(18) Eom, C. B.; Lee, M. K.; Chol, J. H.; Belenky, L. J.; Song, X.; Cooley, L. D.; Naus, M. T.; Patanik, S.; Jiang, J.; Rikei, M.; Polyanski, A.; Gurevich, A.; Cai, X. Y.; Bu, S. D.; Babcock, S. E.; Hellstrom, E. E.; Larbalestier, D. C.; Rogado, N.; Regan, K. A.; Hayward, M. A.; He, T.; Slusky, J. S.; Inumaru, K.; Haas, M. K.; Cava, R. J. *Nature* **2001**, *411*, 558.